Steam Bubble Cavitation

Article *in* AIChE Journal · July 2008

DOI: 10.1002/aic.11509

4 authors, including:

Amit Mahulkar
Ghent University
8 PUBLICATIONS **212** CITATIONS

SEE PROFILE

Aniruddha Bhalchandra Pandit
Institute of Chemical Technology, Mumbai
429 PUBLICATIONS **15,674** CITATIONS

SEE PROFILE

F. Michael Lewis
Innovative Engineering
32 PUBLICATIONS **41** CITATIONS

SEE PROFILE

AIChE

Steam Bubble Cavitation

A. V. Mahulkar, P. S. Bapat, and A. B. Pandit
University Institute of Chemical Technology, Mumbai, India

F. M. Lewis
535 East Mariposa Ave. El Segundo, CA 90245

DOI 10.1002/aic.11509
Published online April 28, 2008 in Wiley InterScience (www.interscience.wiley.com).

Generating hydrodynamic/ acoustic cavitation (Gogate et al.) for a useful purpose encompasses the following energy transformation steps: (1) Burning fuel in boiler. (2) Expanding the steam in a turbine generator. (3) Using electrical output from the generator to: (a) Pump water through a mechanical constriction (hydrodynamic cavitation), or (b) Operate ultrasonic transducer (acoustic cavitation). The combined loss, which is the mathematical product of each of the above step efficiencies, lowers the overall efficiency. An energy efficient method for generating useful cavitation is presented here. It suggests direct injection of steam (I) into sub-cooled water to produce cavitation, thereby eliminating the inefficiencies of the remaining steps (II and III). Cavitation produced by this technique was experimentally and numerically shown to produce collapse conditions similar to hydrodynamic/acoustic cavitation. Direct steam injection cavitation coupled with acoustic cavitation, exhibited 4–16 times greater energy efficiency as compared to acoustic cavitation alone. Similar effects have been numerically speculated for hydrodynamic cavitation. © 2008 American Institute of Chemical Engineers *AIChE J,* 54: 1711–1724, 2008
Keywords: steam cavitation, bubble dynamics, hydrodynamic cavitation

Introduction

Cavitation as a source of concentrated energy input for the chemical processes is increasingly being studied owing to its ability to generate local high temperatures and pressures at nearly ambient bulk processing conditions. Hydrodynamic cavitation have already been applied to several chemical engineering applications (physical and chemical) like water disinfection,[1] waste treatment,[2] oxidation of alkylarenes,[3,4] and emulsification and homogenization.[5] A number of studies made earlier, such as hydrolysis of fatty oils,[6] cell disruption,[7] and polymerization/depolymerization of aqueous polymeric solutions[8] have proved the process to be more energy-efficient than its counterpart, i.e., acoustic cavitation.

Correspondence concerning this article should be addressed to A. B. Pandit at abp@udct.org.

In hydrodynamic cavitation, the cavities or bubbles are generated by the flow of liquid under controlled conditions through simple constricting geometries such as a venturi or an orifice plate. When the pressure downstream of the mechanical constriction such as venturi or orifice falls below the vapor pressure of the liquid, a number of cavities (containing gas/vapor) are generated, which subsequently collapse with the recovery of pressure downstream of the mechanical constriction.

The normal way of creating hydrodynamic and acoustic cavitation consists of the following steps (shown in Figure 1) of energy transformation:

(1) Fuel is burned in a boiler to generate high pressure, high temperature steam.

(2) The steam is expanded in a turbine to provide the mechanical energy to drive an electrical generator.

(3) Electricity thus generated is used to power a motor connected to a pump that pressurizes the water so that it can

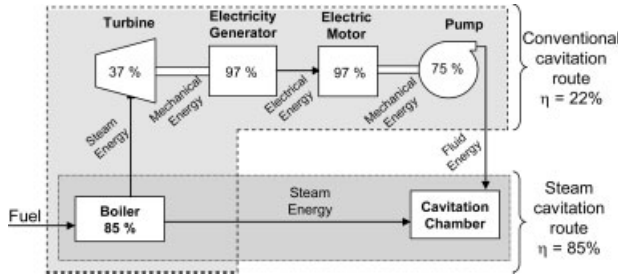

Figure 1. Steam cavitation route and conventional hydrodynamic cavitation route (% indicate the energy conversion efficiency (η) of the step).

pass through a mechanical constriction and create hydrodynamic cavitation. In case of ultrasonic cavitation the electrical energy is given to transducers (through high frequency generator) which generate pressure waves in liquid to create cavitation.

Thus the overall efficiency of the conventional hydrodynamic cavitation process is (boiler 85% $\times$ steam turbine 37% $\times$ electrical generator 97% $\times$ electric motor 97% $\times$ pump 75%) about 22% and in the case ultrasonic cavitation is (boiler 85% $\times$ steam turbine 37% $\times$ electrical generator 97% $\times$ ultrasonic transducers 30%) about 9%. Although ultrasonic transducers with good impedance matching can have conversion efficiency as high as 70%, but still the overall efficiency of ultrasonic cavitation would be 21%. With steam cavitation, steps no. 2 and no. 3 above, along with their respective efficiencies (for the steam turbine, generator, electric motor, and the pump/ultrasonic transducer) are eliminated. Thus overall efficiency of steam-based cavitation is expected to be about (boiler $\sim$85%) 85% (nearly four times more in hydrodynamic cavitation and 9.5 times in acoustic cavitation) and this makes steam cavitation as an attractive option for increasing energy efficiency of the conventional cavitation-based physico-chemical transformations.

Numerical Model for Steam Bubble Dynamics

This section presents the mathematical equations used to model the dynamical behavior of steam bubble when introduced in stagnant and flowing cold water. Here, the dynamics of bubble is modeled using Rayleigh-Plesset equation, developed by Rayleigh[9] and later modified by Plesset[10] and the Tomita-Shima equation.[11] Heat transfer between the liquid and bubble has also been considered which also incorporates the liquid side heat transfer resistance and latent heats of phase change. Mass transfer of condensable vapor to the bulk liquid is also incorporated. Although the numerical models presented here are primarily developed for steam bubble dynamics but they can be readily extended for cavity (vaporous or semi-vaporous) dynamics in case of acoustic and hydrodynamic cavitation also, as has been done successfully earlier.[12]

Dynamics of Steam Bubble

A steam bubble when introduced in a cold flowing liquid experiences a turbulent fluctuating pressure. Similarly, the pressure inside the bubble would change due to the condensation or evaporation of steam as a result of enthalpy transfer due to temperature difference between steam bubble and the surrounding cold water. Such changes in internal and external pressure over a bubble would alter its size. The Rayleigh-Plesset equation (Eq. 1) allows us to estimate the dynamics (change in size with time) of a spherical bubble, placed in an infinite liquid, as a function of changing internal bubble pressure, external liquid pressure, bubble radius, bubble wall velocity and liquid properties like liquid density, surface tension and viscosity without consideration of heat and mass transfer.

$$R(\ddot{R}) + \frac{3}{2}(\dot{R})^2 = \frac{1}{\rho_l}\left[P_B - \frac{4\mu}{R}(\dot{R}) - \frac{2\sigma}{R} - P_\infty\right] \tag{1}$$

Liquid phase Compressibility considerations proposed by Tomita and Shima[11] is represented by Eqs. 2, 3, and 4 and has been considered as the second order approximation to include the effects of the liquid phase pressure on liquid density, enthalpy, and velocity of sound. The liquid phase compressibility becomes significant during the bubble collapse, when bubble wall velocity reaches the velocity of sound in the liquid medium. In the present model Rayleigh-Plesset equation (Eq. 1) is used when bubble wall velocity is less than the velocity of sound (in water it is of the order of 1500 m/s, Mach number < 1) and Tomita-Shima equation (Eq. 2) is used when bubble wall velocity exceeds the velocity of sound (Mach number > 1) to understand and model the cavity (steam bubble) wall motion excluding the heat and mass transfer which are modeled separately. Switching to Tomita-Shima equation from Rayleigh-Plesset equation at Mach number of 0.5 rather than that of 1 showed less than 2% deviation in final collapse pressure and temperature.

$$R\ddot{R}\left(1 - \frac{2\dot{R}}{C} + \frac{23\dot{R}^2}{10C^2}\right) + \frac{3}{2}\dot{R}^2\left(1 - \frac{4\dot{R}}{3C} + \frac{7\dot{R}^2}{5C^2}\right) + \frac{1}{\rho_1}\left[\begin{array}{l} p_{\infty(t)} - p_{2(r=R)} + \frac{R}{C}\left(\dot{p}_{\infty(t)} - \dot{p}_{1(r=R)}\right) + \\ \frac{1}{C^2}\left\langle \begin{array}{l} -2R\dot{R}\left(\dot{p}_{\infty(t)} - \dot{p}_{1_{(r=R)}}\right) + \frac{1}{2}\left(p_{\infty(t)} - \right. \\ \left. p_{1(r=R)}\right)\left(\dot{R}^2 + \frac{3}{\rho_1}\left(p_{\infty(t)} - p_{1(r=R)}\right)\right) \end{array} \right\rangle \end{array}\right] = 0 \tag{2}$$

where P_1 and P_2 as a function of R are given as follows:

$$p_{1(r=R)} = p_B - \frac{2\sigma}{R} - \frac{4\mu}{R}\dot{R} \tag{3}$$

$$p_{2(r=R)} = p_{1(r=R)} - \frac{4\mu}{3\rho C^2}\left(\dot{p}_{\infty(t)} - \dot{p}_{1(r=R)}\right) \tag{4}$$

The above bubble dynamics models are valid for spherical bubble. In case of noncondensing gas bubbles present in the flowing liquid, the viscous stresses tend to make the bubble nonspherical where as the surface forces restore the sphericity of the bubble. But, in case of condensing steam bubble, the sphericity is restored by surface tension force and more dominantly due to high rate of condensation of water vapors in the steam bubble due to the enthalpy transfer to the surrounding cold water. Any nonsphericity coming into the steam bubble increases the surface area to volume ratio of the bubble which in turn increases the rate of heat transfer

and hence the condensation thus removing the distortion from the bubble and making it spherical. This is similar to the grinding effect on nonspherical particle leading to their eventual smoothness and resulting sphericity. High speed photographic results to be discussed later will also show that steam bubble once ejected from the nozzle (after the removal of driving steam pressure effect) immediately gains spherical shape. Thus, the assumption of sphericity of condensing steam bubble is appropriate in this case and the use of Rayleigh-Plesset (Eq. 1) and Tomita-Shima (Eqs. 2–4) equations are justified.

Energy balance over steam bubble

As shown in Figure 2a, three thermal regions are modeled: two in the bubble and third outside the bubble. The steam bubble is divided into two thermal regions. First is central hot core where the temperature (T_B) during the bubble collapse rises adiabatically, second is vapor side cold boundary layer near the interface and the third thermal region is cold liquid side boundary layer. Temperature of bulk liquid (T_∞) is assumed to be constant while the temperature of bubble core (T_B) and bubble liquid interface (T_{in}) is obtained by taking energy balance over the core of bubble and bubble–liquid interface, respectively, which are discussed in the following section.

Prediction of Temperature of Hot Core of Bubble

A general heat balance law can be written as

$$\left\{\begin{array}{l}\text{Rate of}\\ \text{accumulation of}\\ \text{energy}\end{array}\right\} = \left\{\begin{array}{l}\text{Net rate of energy}\\ \text{transfer due to}\\ \text{mass exchange}\end{array}\right\} + \left\{\begin{array}{l}\text{Heat flow in the}\\ \text{control volume}\\ \text{across the surface}\end{array}\right\} + \left\{\begin{array}{l}\text{Net work done on}\\ \text{the control volume}\end{array}\right\}$$

Consider the bubble as the control volume; energy conservation equation can be formulated as

$$\frac{d(mU)}{dt} = \Delta\left[\left(U + \frac{1}{2}u^2 M_{avgw} + zgM_{avgw}\right)\dot{m}\right] + Q + W \quad (5)$$

where U is internal energy of the bubble (J/mol), m is moles of gas inside the bubble (mol), $\dot{m}$ is molal flow in/out of the bubble (mol/sec), Q rate of heat transfer to the bubble from the surrounding and vice versa (J/sec), W is work done on the bubble by the surrounding medium (J/sec). The terms $\frac{1}{2}u^2$ and zg represent kinetic energy and potential energy associated with the incoming/outgoing streams respectively. Since kinetic energy and potential energy associated with the mass entering and leaving the bubble is very small and hence these terms can be neglected at this stage.

The "PV" kind of Work done on the bubble is given by

$$W = P_B dV = P_B d\left(\frac{4}{3}\pi R^3\right) = P_B 4\pi R^2 S \quad (6)$$

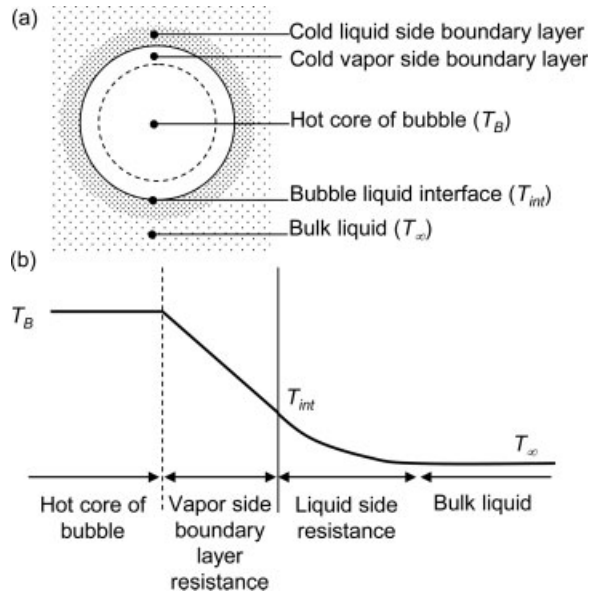

Figure 2. (a) Division of steam bubble into thermal regions; (b) temperature profile across bubble-liquid interface into thermal regions.

The energy carried in by the vaporizing water molecules is given by $U\dot{m} = T_{int}C_v\dot{m}$, where C_v is the specific heat at a constant volume (J/mol K).The vapor entering the bubble due to vaporization is at bubble liquid interface temperature, while the vapor leaving the bubble due to condensation is at inner temperature of the steam bubble (hot core of the bubble).

Toegel[13] and Yasui[14] have modeled the bubble dynamics by assuming all the resistance to heat transfer between the bubble and liquid to be present in the thermal boundary layer inside the bubble. Here in addition to gas side thermal resistance, liquid resistance is also taken into account. Figure 2(b) shows schematically, the temperature profile across the bubble liquid interface and transfer resistances included in the model. Temperature is considered to be spatially uniform in the hot core of the bubble. While, heat transfer from the bubble is controlled by resistance offered by this thermal boundary layer, containing vapor/gas mixture, from which heat transfer takes place due to conduction and is given as

$$Q = 4\pi R^2 K_B \frac{T_{in} - T_B}{l_{th}} \quad (7)$$

The thermal boundary layer thickness l_{th} is given by Toegel et al.[13] as,

$$l_{th} = \text{MIN}\left(\sqrt{\frac{R\alpha_B}{|S|}}, \frac{R}{\pi}\right) \quad (8)$$

where K_B is the thermal conductivity of gaseous (or vaporous) content of the bubble and α_B is the thermal diffusivity. The properties like K_B and α_B are calculated based on the temperature of the bubble–liquid interface and the composition of the bubble i.e. fraction of noncondensable gas.

Prediction of Bubble–Liquid Interface Temperature

When phase change takes place at the interface, latent heat is either liberated or dissipated at the interface. This latent heat is seen as an additional flux in liquid side heat transfer. Taking steady state heat balance over the bubble-liquid interface we get the following equation.

$$\frac{K_B 4\pi R^2}{l_{\text{th}}}(T_B - T_{\text{int}}) - \dot{m}\lambda = h_l 4\pi R^2 (T_{\text{int}} - T_l) \tag{9}$$

Khabeev and coworkers[15] related Peclet number to the Nusselt number for a vapor bubble freely oscillating in liquid as

$$Nu_D = 2 + Pe^{1/2} = 2 + \left(\frac{2R|S|}{\alpha_l}\right)^{1/2} \tag{10}$$

where Nu_D is Nusselt number based on bubble dynamics, Pe is Peclet number, α_l is thermal diffusivity of the liquid, R and S is radius of bubble and bubble wall velocity respectively. Equation 10 is based on the limiting value of Nusselt number for a spherical object in a motionless fluid. The Peclet number term augments the heat transfer coefficient when bubble is oscillating freely (volumetric contraction and expansion) in the liquid. From the above relation we can see that when bubble oscillates, the predicted value of Nusselt number is much greater then 2, thus greatly increasing the heat transfer coefficient and hence the heat flux. Thus, it suggests that the resistance offered by the surrounding liquid to heat transfer is much less (due to bubble oscillations and thermal boundary layer disturbances) in comparison to the gas side heat transfer coefficient. The value of liquid side heat transfer coefficient (h_l) in Eq. 9 is obtained from liquid side Nusselt number which is obtained from Eq. 10.

Mass balance for condensable vapors

Mass transfer of the condensable vapors of the liquid, steam in the present case, has also been considered. If the liquid is pure, there would not be any resistance to mass transfer on liquid side. Thus, all the resistance to mass transfer is offered only by the boundary layer present inside the bubble (possibly due to the presence of noncondensable gas). Mass transfer is seen to be a two step process, first is a phase change at the bubble liquid interface and second is the diffusion of the vapors through the inner gaseous boundary layer in the bubble (in case if noncondensable gases are present in the bubble). In the case of totally vaporous bubble like that in the case of steam bubbles the diffusional resistance in the inner boundary layer is zero. Thus, all the resistance can be attributed to the phase change at the interface.

Based on kinetic theory of gases, model for evaporative mass flux from the interphase was earlier developed by Hertz,[16] Langmuir[17] and Knudsen.[18] Later the model was improved by Schrage[19] and Ytrehus and ϕstmo.[20] The rate of phase change at the gas liquid interface is given as

$$\dot{m} = 4\pi R^2 \alpha_c \sqrt{\frac{1}{2\pi R_g T_{\text{int}} M_v}}(P^O - P_v) \tag{11}$$

where M_{v} is molecular weight of the vapor, P^{O} is the vapor pressure of the liquid at bubble–liquid interface temperature "T_{int}" and P_{v} is the partial pressure of the vapor in the bubble. Equation 11 is based on the kinetic theory of gases. This model takes into account both, the frequency with which vapor molecules collide with the liquid surface (interface) and the probability of the colliding molecule to get condensed on or at the liquid surface. Mass flux equation (Eq. 11) without accommodation coefficient (α_{c}) gives maximum rate at which evaporation or condensation can take place under given pressure or temperature driving force, in absence of any other resistance to mass transfer. The mass flux model originally developed, were based on idealistic assumptions like flat vapor–liquid interface, bulk movement of molecules is normal to the interface etc. Accommodation coefficient accounts for surface curvature, because surface curvature will determine the angle with which vapor molecules collide with the liquid surface (interface) and also its probability of getting condensed. Accommodation coefficient (α_{c}) is introduced to relate the actual rate of mass transfer to the maximum theoretical rate of mass transfer. For water, α_{c} is reported to be equal to 0.35.[14]

Presence of noncondensable gases in the bubble imparts diffusional resistance to the transfer of vapor from gas–liquid interface to the bubble core. Thus, the rate of mass transfer also depends on the diffusional transfer in the inner gaseous boundary layer and is given as

$$\dot{m} = 4\pi R^2 \frac{D_{AB}}{l_{\text{th}} R T_{\text{int}}}\left(P^O - P_v\right) \tag{12}$$

Similar to heat transfer boundary layer, the mass transfer boundary layer thickness has been calculated using following equation (Eq. 13)

$$l_{\text{m}} = MIN\left(\sqrt{\frac{RD_{AB}}{|S|}}, \frac{R}{\pi}\right) \tag{13}$$

Overall mass transfer rate is based on both the resistances which will be discussed later while finalizing the model equations.

Effect of fluid turbulence in flowing liquids

The fluid turbulence (*rms* fluctuating velocities) present typically in flowing liquids affects the bubble dynamics in the following ways.

The Turbulent Fluctuating Pressure. The turbulent fluctuating pressures due to turbulent fluctuating velocities in the flowing liquid near the bubble affect the bubble dynamics. Model presented by Moholkar and Pandit[21] for obtaining the turbulent fluctuating pressure downstream the orifice is used here. Turbulent instantaneous pressure variation is correlated to geometrical parameters like pipe size and orifice size and to the operating parameters like liquid pressure and velocity at orifice. Details of calculations of turbulent pressure variation for a particular case (cavitation number =1) is given in Appendix A.

In a typical example of water flowing through a pipe (without cavitating device i.e. orifice) at 1 m/s with turbulent intensity as high as 20%,[22] the fluctuating velocity works out

to be 0.2 m/s. The Turbulent fluctuating pressure can be related to the fluctuating velocity as

$$P' = {}^{1}\!/_{2}\rho v'^{2} \tag{14}$$

where P' is the turbulent fluctuating pressure, which is the dynamic pressure of turbulent fluctuating velocity v'. Thus, the corresponding magnitude of the fluctuating pressure is 20 Pa, which is much less in magnitude to cause any significant change in the bubble dynamics. Thus, the effect of turbulent pressure fluctuations is neglected when steam bubble is introduced in water flowing through a pipe without orifice, venturi or a nozzle. However, the pressure fluctuations can be substantially higher, i.e. in order of 20,000 Pa, near a cavitation device like orifice, venturi, or a nozzle and cannot be neglected when accounting for dynamical changes in the steam bubble. In this article numerical simulation for steam bubble being introduced in stagnant pool of cold water, in sonicated pool of cold water and in cold water flowing through a standard hydrodynamic cavitation device i.e. orifice[23] have been presented.

The Turbulent Shear Stress Limits the Size of Bubble. The turbulent fluid shear stress limits the maximum size of the bubble that can remain stable and can be introduced through the steam injection nozzle. The Weber number criterion is used to relate the maximum size of the bubble to the turbulent fluctuating velocity.[24] Maximum size attended by bubble is restrained by critical Weber number (We) and the criterion is defined as (based on orifice flow).

$$We = \frac{2Rv'^{2}\rho}{\sigma} = 4.7 \tag{15}$$

When the bubble size becomes greater than critical size (as a result of mass/vapor diffusion or pressure variation) given by Weber number, than the bubble size reduces (by break-up) to critical size due to turbulent shear.

Turbulence Enhances the Liquid Side Heat Transfer Coefficient. Heat transfer from a stationary sphere placed in the flowing liquid is well established. One such correlation is given by Whitaker[25]

$$Nu_{\mathrm{T}} = 2 + \left(0.4Re^{1/2} + 0.06Re^{2/3}\right)Pr^{0.4}\left(\frac{\mu_{\infty}}{\mu_{\mathrm{in}}}\right)^{1/4} \tag{16}$$

where Nu_{T} is Nusselt number based on turbulent flow past over a spherical bubble, Re is Reynolds number, Pr is Prandtl number, μ_{∞} is viscosity of liquid based on bulk temperature of liquid and μ_{int} is viscosity of liquid based on bubble–liquid interface temperature. It relates the Prandtl number and Reynolds number based on relative velocity between the bubble and liquid to the Nusselt number. While discussing the predictions of bubble–liquid interface temperature in earlier section, Nusselt number based on bubble oscillations has been discussed (Eq. 10). Both the Nusselt numbers based on bubble oscillations (Eq. 10) and liquid turbulence (Eq. 16) are compared here and the higher one is used to calculate the maximum liquid side heat transfer coefficient.

In the following section details of the experiments with steam injection will be given. The results of the experiments will be discussed on the basis of simulation results of the model developed in this section.

Final form of model

We now rewrite the equations for bubble dynamics, heat transfer and mass transfer in their final form as,

Bubble Dynamics. This gives radius (R) and bubble wall velocity (S) as a function of time. Based on the bubble wall velocity, either Rayleigh-Plesset equation (Eq. 1) or Tomita-Shima equations (Eqs. 2–4) have been used to estimate the history of cavity size.

When $S < 1500$ m/s Rayleigh-Plesset equation (Eq. 1) is used.

When $S > 1500$ m/s Tomita-Shima equation (Eqs. 2–4) is used.

Mass Transfer Equation. Adding the two resistances, i.e., diffusion resistance and resistance based on kinetic theory gives the following combined equation

$$\dot{m} = 4\pi R^{2}\frac{P^{\mathrm{O}} - P_{v}}{\left(\frac{D_{\mathrm{AB}}}{l_{\mathrm{th}}RT_{\mathrm{int}}}\right)^{-1} + \left(\alpha_{c}\sqrt{\frac{1}{2\pi R_{g}T_{\mathrm{int}}M_{v}}}\right)^{-1}} \tag{17}$$

The boundary layer thickness l_{th} is obtained from Eq. 13 and diffusivity of water vapor in noncondensable gas is calculated based on molecular theory of gases.[26]

Energy Balance. For temperature inside the bubble (T_{B}) combining the Eqs. 5, 6 and 7 we get

$$\frac{d(mCvT)_{B}}{dt} = 4\pi R^{2}K_{B}\frac{T_{\mathrm{int}} - T_{B}}{\min\left(\sqrt{\frac{R\alpha}{|S|}}, \frac{R}{\pi}\right)} - P4\pi R^{2}S + \left\{\begin{array}{ll} \dot{m}(CvT)_{\mathrm{int}} & \dot{m} > 0 \\ \dot{m}(CvT)_{B} & \dot{m} < 0 \end{array}\right\} \tag{18}$$

For temperature at the bubble–liquid interface (T_{int}) based on steady state rate (Eq. 9) we have

$$\frac{K_{B}4\pi R^{2}}{l_{\mathrm{th}}}(T_{B} - T_{\mathrm{int}}) - \dot{m}\lambda = h_{l}4\pi R^{2}(T_{\mathrm{int}} - T_{l}) \tag{19}$$

to determine the liquid side heat transfer coefficient we use maximum of two Nusselt numbers, one based on turbulent cross flow over the spherical bubble (Nu_{T}) (Eq. 18) and other based on oscillations of bubble (Nu_{D}) (Eq. 10)

$$\frac{h_{l}(2R)}{K_{l}} = MAX\left(Nu_{D}, Nu_{T}\right) \tag{20}$$

Termination Criterion. Cavity collapse criterion is based on material volume concept. Van der waals equation of state is given as

$$\left(P - \frac{an^{2}}{V^{2}}\right)(V - nb) = nRT \tag{21}$$

Where, "n" is number of moles and "b" is the measure of excluded volume per mole of gas and can be regarded as the material volume per mole of gas. Therefore any gas cannot be compressed beyond its material volume which is given as "bn". Once the bubble volume reduces to the material volume of molecules (bn) present in it bubble is said to be collapsed. At the end of each time step, the material volume of the then bubble content is calculated and compared to its

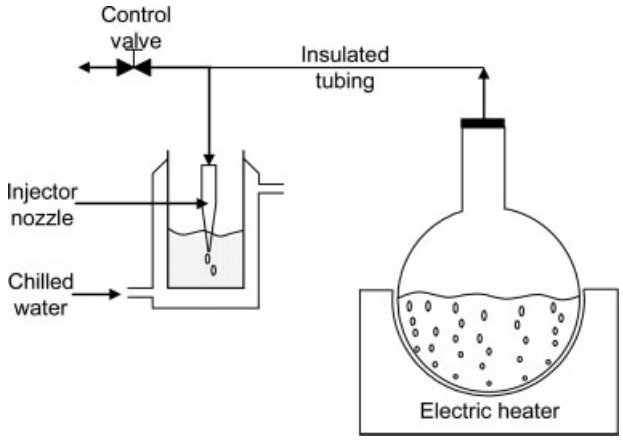

Figure 3. Experimental setup for KI decomposition by steam cavitation.

actual volume. Simulation is terminated as soon as actual volumes equals or becomes lesser than material volume.[27]

Numerical Method. The model has three ordinary differential equations, for R, S (Eq. 1 or 2) and T_B (Eq. 20) and two algebraic equations, for T_{int} (Eq. 21) and $\dot{m}$ (Eq. 19) which need to be solved simultaneously. The algebraic equations can be merged into one to be solved by secant method. Runge Kutta 4th order method is used to solve the ODE's. For simulation purpose at time $t = 0$, i.e. at time of detachment of steam bubble from steam jet, the steam bubble is assumed to be in mechanical equilibrium with surrounding liquid. Thus, the pressure inside the steam bubble is taken as Laplacian stress developed inside the bubble due to surface tension. Initial bubble wall velocity is taken as zero and the temperature of steam inside the bubble is taken as same as that of incoming steam.

Experiments of Steam Cavitation in Cold Water Pool

It is first necessary to observe, whether the cavitation (in a sense of its conventional definition) actually occurs due to condensing/collapsing steam bubble in cold water. For this purpose oxidation of potassium iodide (KI) to form Iodine is considered as a model reaction. Weissler et al.[28] and Naidu et al.[29] have shown that the decomposition of aqueous solution of KI is attributed to the generation of strongly oxidizing $OH^{\bullet}$ radicals. The generation of $OH^{\bullet}$ radicals from dissociation of water is possible only under extreme conditions of temperature and pressure, which are generated locally in cavitation phenomena, as a result of violent cavity collapse. It means that the decomposition of aqueous KI can't occur only by the fluid shear, impact or rapid pressure variations in flowing liquid or just by heating the KI solution (thermal degradation) and cavitation conditions is very much essential for the same. In present study blank trials, discussed later, were performed to indicate that KI decomposition does not occur due to boiling or heating it to temperature of saturated steam.

Steam injection in stagnant water pool: effect of pool temperature

The experimental setup is shown in Figure 3. Steam is produced by boiling distilled water. Steam was taken through the insulated tubing to a converging plastic nozzle with an exit diameter 0.75 mm.

Distilled and degassed water was used to make aqueous solution of KI (5% w/v). Degassing was done by boiling the distilled water for ~10 min. Degassing of water is very important in steam cavitation experiments, because, on introducing steam in a nondegassed aqueous solution, the gases dissolved in water are desorbed into the steam bubble. Desorption of gases into steam bubble is facilitated by increased temperature of liquid surrounding the steam bubble which decreases the solubility of gases in this water film surrounding the steam bubble. The gases dissolved in the water diffuse into the steam bubble also because of the partial pressure of gas inside the steam bubble being lower than its equilibrium partial pressure for given dissolved concentration of gas in water. At the time of collapse or rapid condensation of a steam bubble, the noncondensable gases entered into the bubble impose very high mass transfer resistance for steam to condense and hence they not only reduce the intensity of collapse but also resist the bubble from reaching the final stage of complete collapse. In the present case, while conducting experiments of introduction of steam into nondegassed water pool, the water became hazy due to desorption of gas and formation/ accumulation of bubbles of noncondensable gases could be observed as per the above discussed hypothesis.

Experiments were conducted at different water pool temperatures i.e. 30, 40, 50, 60, and 70°C. Chilled water was circulated through the outer jacket of the vessel to maintain the pool at a desired temperature. About 50 mL aqueous KI was taken into the beaker in which steam was introduced for 20 min. The steam flow rate was measured by making the steam completely condense in cold water and then measuring the weight gained by the water due to steam condensation. The steam flow rate was measured to be 26.6 mg/s.

Iodine liberation analysis was done with UV-Visual spectrophotometer at a wavelength of 354 nm to measure absorbance. With the help of calibration data (Figure 4) of iodine

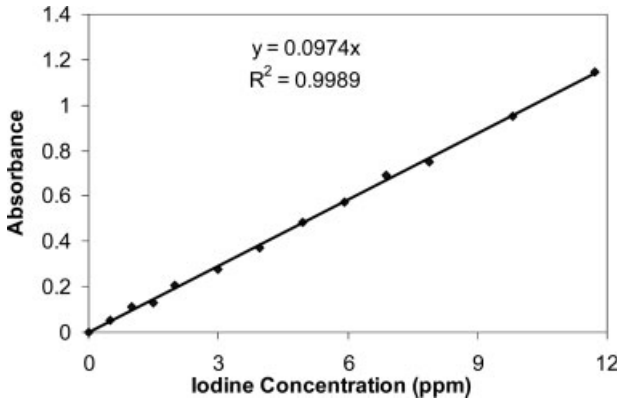

Figure 4. Calibration chart of Iodine absorbance at different Iodine concentration.

concentration and the absorbance, the amount of iodine liberated was calculated and the extent of degradation of KI in each run was obtained.

Results and Discussions

To confirm that the KI degradation occurred only because of cavitational effects produced by collapse of steam bubble and not by rise in temperature due to introduction of steam or by any other unknown factor two blind trials were conducted. In first blind trial, the same concentration (5% w/v) and same volume of KI solution (50 mL) was kept for 20 min in the set-up without introduction of steam; still no Iodine was detected in the KI solution which means that no KI degradation occurred in absence of cavitation. In second blind trial, the pressure over the KI solution was raised to 2 atmg and then the KI solution was heated to 100°C (boiling point of water at 2 atmg is 133.3°C). KI solution was kept at 2 atmg and 100°C for 20 min, after which the solution was first brought to room temperature than the pressure was brought back to atmospheric pressure. No iodine was detected in the KI solution which proves that even at 100°C no thermal degradation of aqueous KI is seen. Thus the Iodine which is detected can be surely said to be formed from cavitational oxidation of KI on introduction of steam.

Figure 5 shows the extent of degradation of KI at various pool temperatures by introduction of steam for 20 min at 26.6 mg/s in 50 mL of aqueous KI solution. As said earlier for the degradation of KI we need to produce $OH^{\bullet}$ radicals which is only possible under cavitating conditions and hence it is shown experimentally that introduction of steam bubbles in sub-cooled water creates cavitational effects due to the violent collapse of steam bubbles. The explanations of variations in the extent of degradation of KI (extent of iodine released) with liquid pool temperature will be given on the basis of simulated dynamics of steam bubble, photographic study of steam injection in pool and direct steam condensation regime map later.

Photographic Study

Injection of steam in stagnant cold water pool was photographed using a high speed camera at 10,000 frames per second (fps). Figure 6 shows the photographs of steam injection

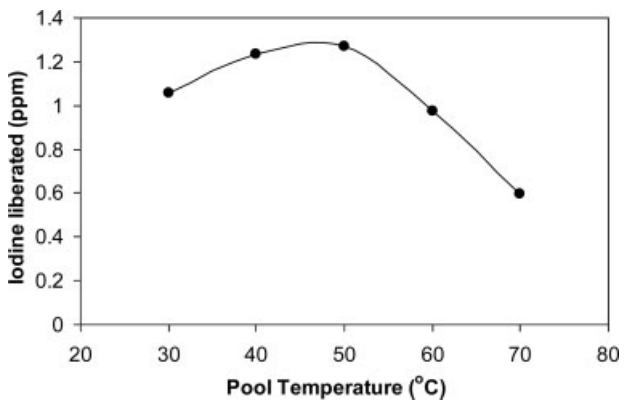

Figure 5. Iodine liberated from degradation of KI.

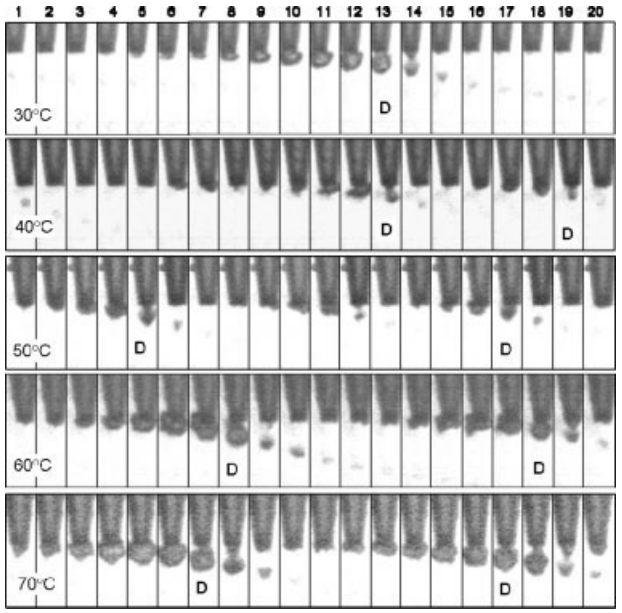

Figure 6. High speed images of steam injection for various pool temperatures.

(Time interval in each image is 100 μs).

at 26.6 mg/s into the water pool at 30, 40, 50, 60, and 70°C. The time interval for each subsequent image is 100 μs. In figure 6, frames marked with "**D**" shows the steam bubble either "just detached" or "just to be detached" from the nozzle.

It can be seen from the high speed images of steam bubble that most of the steam bubbles that detach from the nozzle (frames marked with "**D**") are spherical on detachment. As said earlier, the high rates of condensation remove the non-sphericity in the bubble. This can be particularly seen in 12th and 13th frame of second row of images (40°C). A highly elliptical bubble is seen to be formed in 12th frame, but as soon as the bubble is detached it is seen to become spherical (frame 13th). Hence, for modeling the dynamics of condensing steam bubble the assumption of sphericity is justified.

Figure 7 is the regime map for direct condensation of steam in water at atmospheric pressure. Different regimes of steam condensation, which essentially discusses steam jet formation and breakup mechanism with respect to steam flux and pool temperature, are identified by many researchers.[30–32] The mechanism of steam bubble/ jet formation is based on relative rates of momentum of steam (steam flux) and rate of condensation of steam. When the momentum (steam flux) associated with the steam is high enough to push the liquid water away it forms the longer steam (vaporous) jet but the stability of the jet i.e. the time required for the breakup of steam jet into steam bubble depends on the rate of condensation which in turn depends on temperature difference between the steam and the surrounding water.

In the present case, experiments were done at steam flux of 60.2 kg m^{-2} s^{-1} (26.6 mg/s through 0.75 mm nozzle). In this work the regime map presented by Chun et al.[32] is taken as a reference for explaining steam condensation phenomena based on the steam flux and pool temperature. We can find from the regime map (Figure 7) that the steam condensation in the present case was occurring either in chugging regime

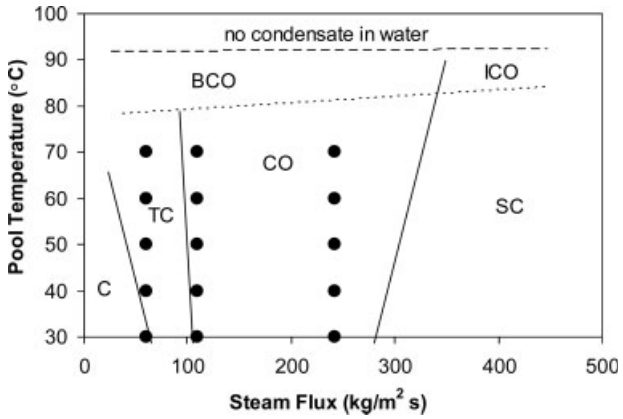

Figure 7. Regime map for direct steam condensation in sub-cooled water (Chun et al., 1996) C, chugging; TC, transient chugging; CO, condensation oscillation; SC, stable condensation oscillation; IOC, interfacial oscillation condensation; BCO, bubbling condensation oscillation.

The filled circles (●) indicate region at which experiments were conducted in present case.

(C) or in transient chugging regime (TC) depending upon water pool temperature.

The "chugging" (C) regime (periodic build-up and collapse of steam plumes) occurs at low liquid temperature and low steam flux (~60 kg/m^2 s). In this regime, the steam water interface progresses beyond the nozzle exit and a small cylindrical steam region is formed there. However, immediately after the formation of the cylindrical bubble, the surrounding water rushes towards the steam plume region. This rush of water towards the steam plume region cuts off the steam supply and detaches a steam bubble. The detached steam bubble immediately collapses due to high rate of condensation. The subcooled water then rushes into the nozzle due to the negative pressure generated by a sudden condensation of bubble. The steam pressure inside the nozzle builds up which pushes the water out of the nozzle. With the momentum of the out-flowing water a small steam is drawn out of the nozzle which further breaks into the bubble and the cycle continues. The chugging regime is characterized by very low frequency of steam bubble formation. In the present case the chugging regime is observed when liquid pool temperature is 30°C. Images of the steam bubble ejection on this regime is shown in first row in Figure 6.

In transient chugging regime (TC), the subcooled water does not enter the nozzle any more. Instead, continuous ejection of steam takes place from the nozzle. The steam coming out of the nozzle immediately breaks into the bubble possibly due to Rayleigh-Taylor instability. As the temperature of pool increases, larger steam bubbles are formed due to lower rate of steam condensation. At higher temperatures (~70°C) the steam bubble partly grows above the nozzle exit due to buoyancy and begins to encapsulate (envelope) the tip of the nozzle. This growth period is followed by the detachment of steam bubble from the nozzle which is now grown large enough to become unstable. Images of steam bubble formation transient chugging regime (TC) is shown in Figure 6 (liquid pool temperature 50°C and 70°C). The size of ejected steam bubble and frequency of bubble ejection for various liquid pool temperatures is given in Table 1.

Table 1. Size of Steam Bubble at the Time of Detachment and Detachment Frequency of Steam Bubbles for Different Pool Temperatures

Liquid Pool Temperature (°C)	Average Diameter of Steam Bubble at the Time of Detachment (mm)	Number of Steam Bubbles Per Unit Time (s^{-1})
30	1.42	615.60
40	1.36	1427.14
50	1.52	1531.53
60	1.83	984.10
70	2.21	890.00

From Figure 5 it is seen that the extent of KI decomposition exhibits a maxima between 40 and 50°C. For liquid pool temperature above 50°C the extent of KI decomposition decreases with an increase in the liquid pool temperature. The cavitational yield of the process depends on collapse intensity of individual bubble and the total number of bubbles collapsed. Figure 8 shows the calculated collapse pressure and temperature for steam bubble introduced in water pool kept at different temperatures. The initial sizes of steam bubble used for simulations were those obtained from the photographic analysis described earlier in this section (Table 1). With an increase in the liquid pool temperature the vapor pressure of the water increases and hence the vapor content of the steam bubble during final collapse conditions also increases. Thus, more mass is compressed at the time of collapse and hence we get an increase in the collapse pressure and temperature with an increase in liquid pool temperature. Toegel and Lohse[33] have shown that collapse temperature of 4000 K is sufficient for the dissociation of several chemical species including water. From Figure 8 it can be seen that collapse temperature for all the cases of steam bubble collapse in the present case are near or greater than 4000 K. Thus, for all the liquid pool temperature considered here the collapse of steam bubble generates OH*. Hence the variation in the extent of KI decomposition for different liquid pool temperature is not controlled by the collapse intensity of

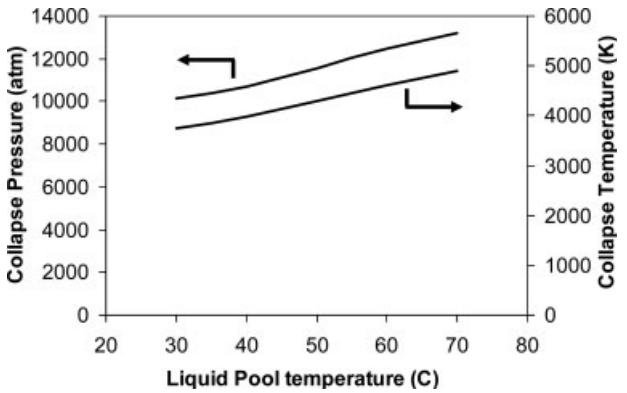

Figure 8. Numerical predictions of collapse pressure and temperature for steam bubbles as function of liquid pool temperature.

individual bubbles but by the number of cavitational events (steam bubbles) introduced in the KI solution.

Table 1 show the number frequency of steam bubble which were measured experimentally from the photographic study. It can be seen that the number frequency of bubble and extent of KI degradation follows the same trend. Highest bubble frequency and KI degradation is seen around 40–50°C.

Steam injection in stagnant water pool: effect of steam flux

Steam cavitation was also studied at different values of steam fluxes. The experimental setup was same as described in previous section. In these experiments the steam nozzle of 1.25 mm was used. The experiments were conducted at three different steam fluxes 58, 109, and 242 kg/m^2 s. The three steam fluxes were chosen so as to study steam induced cavitation in different regimes of condensation, namely chugging (C), transient chugging (TC) and condensation oscillations (CO). Experiments could not be conducted in stable condensation regime (SC) due to difficulties aroused in maintaining the liquid pool at constant and required temperature at high steam fluxes. The three steam flowrates were for above mentioned steam fluxes are 71.2, 134, and 297 mg/s. In all the experimental runs 100 mL of aqueous solution of KI (1% w/v) prepared in distilled and degassed water was taken into a jacketed vessel. To maintain the temperature of the liquid pool to a desired temperature the steam was introduced intermittently into the solution. In each run 200 g of steam was introduced into the KI solution.

Results and Discussions

Figure 9 compares the final quantity of iodine liberated for three different steam fluxes and five different pool temperature. It is seen that for all the values of steam flux the extent of iodine liberation is highest when pool temperature is maintained between 40 and 50°C as previously observed in previous section. From Figure 9 it can also be seen that the quantity of iodine liberated is highest at low steam flux (58 kg/m^2 s) as compared to higher steam fluxes. According to the condensation regime map (shown in Figure 7) for low steam flux (58 kg/m^2 s) the condensation regime is chugging (C) and transient chugging (TC) In this regime individual steam bubbles are continuously issued from the steam nozzle which collapse in surrounding water. When steam flux is 109 and 242 kg/m^2 s the regime is condensation oscillation (CO). In this regime, the steam condenses outside the nozzle and the steam-water interface oscillates violently and the ambient water moves back and forth according to the plume motion. In this regime the bubble detachment from steam nozzle takes place after a few oscillations which delay the bubble detachment process. This results into lesser number of steam bubbles from a given mass of steam (steam flux). Thus the overall cavitational yield is lesser than in the case of lower steam flux (regime "C" and "TC").

Cavitation regimes in condensation regime map

From the experimental results presented in previous section, it can be conclusively said that injection of steam into

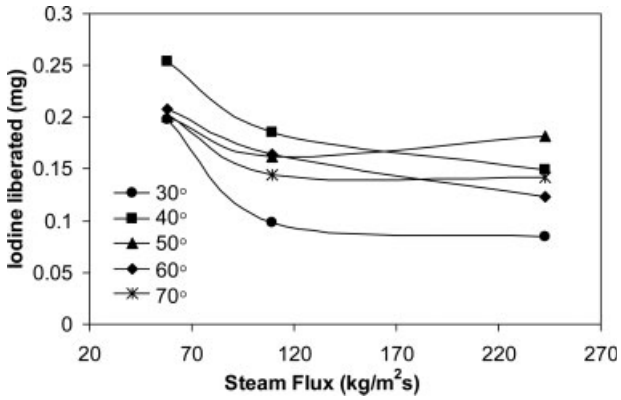

Figure 9. Experimental quantification of extent of iodine liberation for various steam fluxes and liquid pool temperature.

stagnant pool of subcooled liquid creates cavitational events. Based on the direct contact condensation regime reported in the literature, the mechanism of condensation was understood and the same was extended to understand the process of steam bubble formation and its collapse which results into the cavitational event. Figure 10 shows cavitational regimes superimposed on condensation regimes map. Various cavitational regimes are categorized based on the amount of Iodine liberated for various steam fluxes and liquid pool temperature. It is seen that the cavitational activity was highest when liquid pool was at the temperature range of 40 to 50°C and for 58 kg/m^2 s of steam flux (TC). Overall the cavitational yield was highest in transient chugging (TC) condensation regime as compared to any other condensation regimes. In case of stable condensation (SC) regime the steam condensation occurs in the form of a stable steam jet (condensation from cylindrical jet surface) without formation of steam bubbles and hence it can be said that no cavitation takes place in stable condensation regime.

Several applications involve heating by direct injection of steam into the material. In such case cavitation occurring due to condensation of steam may not be desirable. Steam injection nozzles can be designed and operated in noncavitating regimes, Stable Condensation (SC), based on the above cavitation regime map.

Steam Assisted Ultrasonic Cavitation

Experiments were also conducted to quantify the extent of improvement in cavitational yield of ultrasonic cavitation by injection of steam. Experimental setup is same as that described earlier (Figure 3), except that the 100 mL KI solution (5% w/v) was taken in conical flask which was placed in an ultrasonic bath. For comparison of energy efficiency of steam cavitation and acoustic cavitation experiments were carried out with steam injection only, sonication only and with combination of steam and sonication. The KI solution (5% w/v) was prepared in degassed as well as nondegassed water to study the effect of initial nuclei on overall cavitational yield. In all the cases the same material content (KI solution) was used and maintained at constant temperature of 30°C throughout the run time. The steam flow rate in the

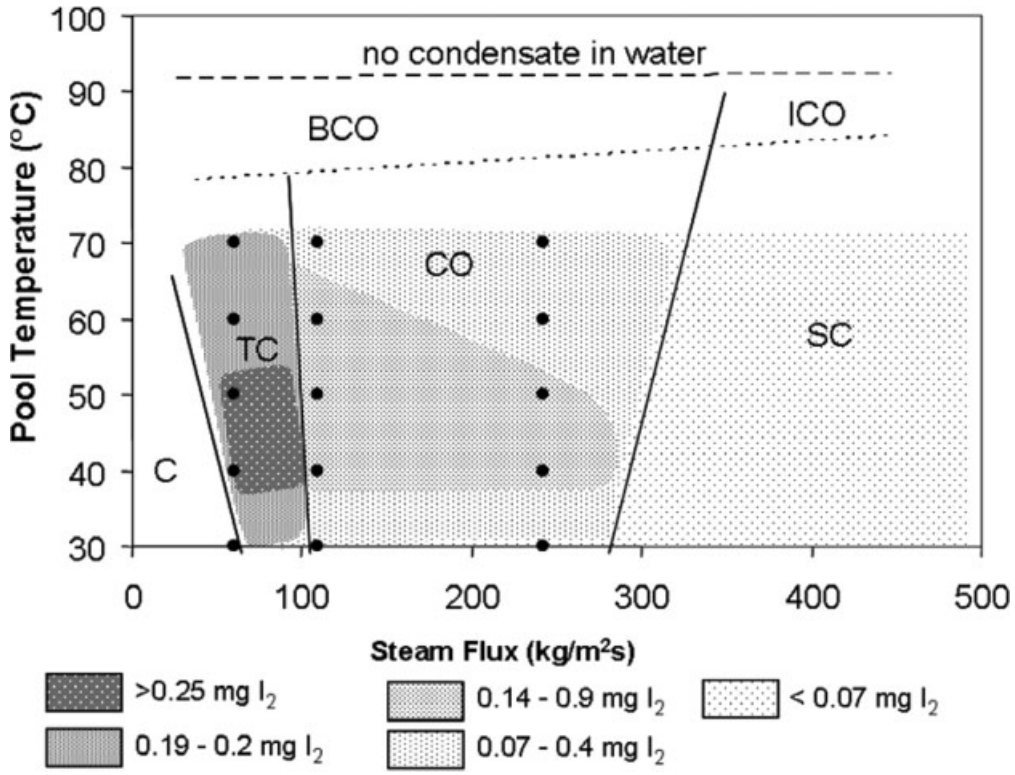

Figure 10. Cavitation regime map superimposed on condensation regime map. Cavitational regions categorized on the basis of amount of iodine liberated.

relevant cases (II, III, and V, shown in Table 2) was 26.6 mg/s. The steam was injected through the nozzle with exit diameter of 0.75 mm.

Figure 11 shows the extent of Iodine liberation for various cases of steam and acoustic cavitation. As can be seen from Figure 11 the extent of KI degradation in the case of degassed water with sonication alone (Case I) is negligible. This is expected because of two reasons. Firstly, since the degassed water is used, the number of initial nuclei (dissolved gases) present in the KI solution is very small. Secondly, the energy delivered to the system (22 W, power intensity = 0.1 W/cm^2, Pressure amplitude = 54,772 Pa) is not sufficient to generate new cavities in KI solution in absence of dissolved gas. In the case of sonication alone in nondegassed liquid (case IV) a marginal increase in KI degradation is seen. Since the acoustic energy delivered to the system is same in both the cases (I and IV), the increase in the extent of KI degradation, in Case IV, is purely attributed to the additional nuclei that are present in the nondegassed water. Nucleation occurring during cavitation is a strong function of dissolved gases present in the liquid.[34] Solubility of air at 25°C in water is 23 ppm.[35] In the present case, the solubility of dissolved oxygen in degassed water was measured using a OXI340i dissolved oxygen meter and was found to be 2.5 ppm (complete degassing has not occurred). This minimum solubility corresponds to the solubility of air in boiling water. The solubility of oxygen in water is higher than the solubility of nitrogen. Air dissolved in water contains ~35.6% oxygen compared to 21% in air. Thus the dissolved air in degassed water is found to be (2.5/0.356) 7.024 ppm. The ratio of dissolved air in nondegassed water and degassed water is (23/7.02) 3.27, where as the ratio of extent of Iodine liberation from nondegassed KI solution and degassed KI solution is also found to be (0.0123/0.00037) 3.24. This clearly indicates the dominant role of dissolved gases in providing nuclei for cavitation to take place and can be used to estimate the cavitational yield for a given energy input.

Table 2. Energy Efficiency Comparison

Case	Type of Cavitation	Steam Flowrate (mg/s)	Acoustic Power (J/s)*	Enthalpy Associated with Steam (J/s)**	I_2 Liberated (mg) in 25 min	Energy/mg of I_2 (kJ/mg)
I	Sonication	–	22	–	0.0037	8688.0
II	Steam	26.6	–	68	0.0512	1991.1
III	Sonication + Steam	26.6	22	68	0.2542	530.9
IV	Sonication	–	22	–	0.0123	2678.8
V	Sonication + Steam	26.6	22	68	0.1624	831.2

*Acoustic power delivered to the system based on calorimetric efficiency (18.33%) maximum power 120 W.
**Enthalpy given by saturated steam at 105°C when condensed & cooled to liquid water at 25°C.

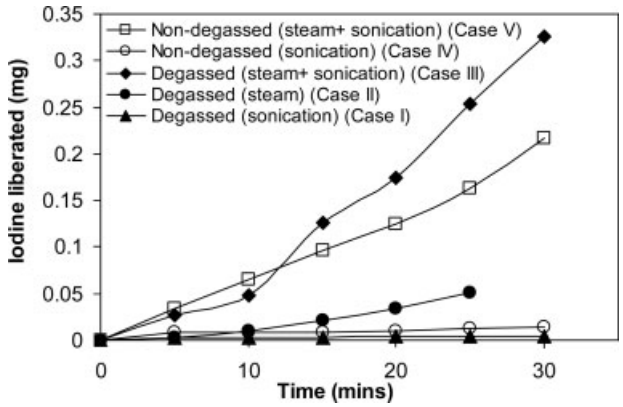

Figure 11. Extent of Iodine liberation for different cases of steam and acoustically induced cavitation.

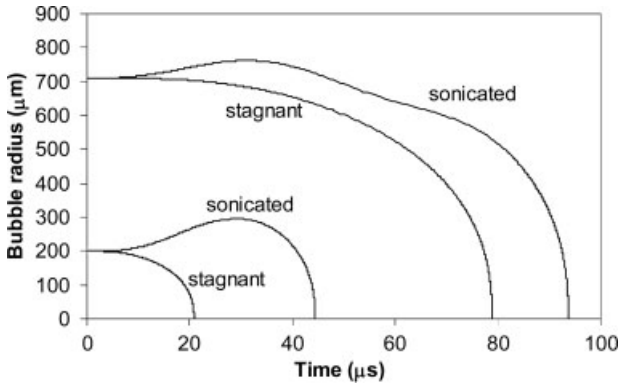

Figure 12. Simulated bubble dynamics of steam bubble induced in stagnant liquid pool and sonicated liquid pool.

In the case of steam injection along with sonication (Cases III and V) the extent of KI degradation is seen to be substantially higher as compared to other cases of sonication or steam injection alone. Table 2 compares the energy efficiency of the cavitation process for various cases. It is seen that energy efficiency of steam assisted sonication is 16 times greater than that of sonication alone for degassed case (Case I) and four times more energy efficient for nondegassed case (Case IV). This proves, experimentally, that the steam induced cavitation works synergistically with acoustic cavitation to improve the overall yield of the cavitation process.

Figure 12 shows the dynamics of the bubble of two different size under stagnant (silent) and sonicated conditions (ultrasound frequency 22 kHz, intensity 2 W/cm^2). It can be seen that the dynamics of larger steam bubble (initial radius 710 μm) is not much affected by the fluctuating pressure and hence the final stage of collapse is more or less similar in both, sonicated as well as stagnant (silent) liquid pool. The collapse pressure of large steam bubble (710 μm) for sonicated and stagnant (silent) was found to be 10,734 and 10,479 atm respectively. On the other hand, the dynamics of smaller steam bubble (initial radius 200 μm) changes drastically when sonicated. The collapse pressure of the smaller steam bubble for sonicated and stagnant (silent) case was found to be 8898 atm and 7506 atm respectively. Thus further improvement in the efficiency of steam assisted ultrasonic cavitation is possible by introducing smaller steam bubbles in the system. Smaller steam bubble can be generated by using steam nozzle of smaller dimension. However, care should be taken that the steam flux remains in transient chugging (TC) regime for maximum bubble ejection frequency.

Steam Bubble Dynamics Near Hydrodynamic Cavitating Device

Consider the saturated steam at a temperature equal to its saturation temperature at the operating pressure of the pipe is injected immediately after the cavitating device i.e. orifice at its vena contracta as shown in Figure 13. A cylindrical pipe of 38 mm ID with orifice plate with 1 number of 5.5 mm diameter hole is considered for simulations.

A dimensionless parameter which has been widely used in the study of hydrodynamic cavitation is the cavitation number,[36] which is defined as

$$C_{vn} = \frac{P_2 - P_{vena}}{1/2 \rho V_{vena}^2} \tag{22}$$

Cavitation number is a theoretical scale to measure the inception and extent of cavitation. For cavitation to occur cavitation number should be equal to or less than 1. Lesser the cavitation number, greater will be the extent of cavitation. Here, two values of cavitation numbers are simulated (1 and 2). Cavitation number equal to and greater than 1 are selected because as said earlier, by the introduction of steam bubble it is not necessary to reach the real cavitating conditions (cavitation number < 1) as we are already providing the fully grown cavity at vena contracta. The turbulent fluctuations seen by the cavity is modeled as discussed earlier. The flow parameters like velocity at the orifice, turbulent velocity and pressure fluctuations for chosen cavitation number and orifice geometry are given in Table 3 (sample calculations given in Appendix A).

Figures 14 and 15 shows radius history of 50 μm, 100 μm and 200 μm initial radius of steam bubble introduced after the cavitating device for cavitation numbers 1 and 2 respectively. It is seen that for a given cavitation number and for various values of initial bubble sizes the radius history is almost similar only after a critical maximum value of the initial radius. This critical radius is the maximum stable size of

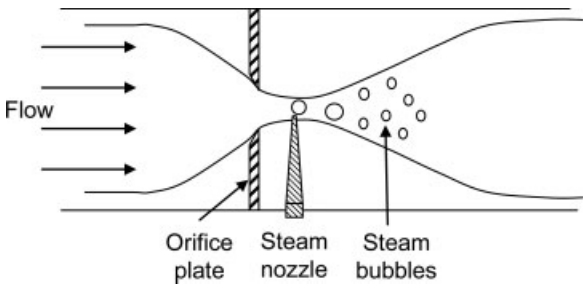

Figure 13. Steam injection after cavitating device.

Table 3. Flow Parameters at Cavitating Device at Different Cavitation Numbers

Cavitation Number	Velocity @ orifice (m/s)	Turbulent fluctuating velocity (m/s)	Turbulent fluctuating pressure (N/m^2)	Turbulence frequency (Hz)
1.0	22.4	0.76	12037	440
2.0	15.8	0.68	6646	394

a bubble in a given fluid turbulence level, defined by the Weber number criterion, which is discussed earlier. Since the cavity dynamics is same for different initial sizes of bubble at a given Cavitation number, the collapse pressure and temperature are also the same. Table 4 shows the final collapse pressure and temperature for various initial sizes of steam bubbles introduced after the cavitating device operated at various cavitation numbers.

The magnitudes of collapse pressure are seen to decrease with an increase in cavitation number. This is because of the fact that the turbulence frequency decreases with an increase in the Cavitation numbers (as shown in Table 3), hence the cavity collapse takes place over a relatively longer time. The increase in the time of collapse of steam bubble with an increase in cavitation number can also be seen from Figure 14 and 15 (142 μs and 180 μs for cavitation number 1 and 2, respectively).

It is seen that whatever size of steam bubble is injected after the cavitating device, the fluid shear in the flow reduces the bubble to its maximum stable size (limited by critical Weber number criteria), and hence does not show any influence of initial bubble size. Thus, by properly selecting the operating Cavitation number we can achieve the required size of the sheared (stable) steam bubble from the nozzle and hence possibly the needed cavitational yield with optimal use of steam. Experimental work is currently being carried out and will be published later.

Conclusions

Steam cavitation route is seen to be much more energy efficient as compared to the conventional cavitation. This is because of the elimination of intermediate energy-interchange processes, like steam energy to mechanical energy (steam turbines), mechanical to electrical energy (electricity generator) and electrical to fluid energy (electric motor and pump/ ultrasonic transducer).

In steam cavitation, steam is directly introduced in liquid water. These steam bubbles act as an expanded cavity which further collapses violently in cold liquid. These steam bubbles directly introduced in the cold water were numerically and experimentally shown to cavitate, producing intense collapse conditions. Numerical model is developed to relate and predict the steam bubble dynamics and collapse conditions with operating parameters like initial bubble size, liquid pool temperature.

Steam assisted ultrasonic cavitation were seen to be almost 4 to 16 times more energy efficient than conventional acoustic cavitation. Steam bubble introduced in sonicated liquid is seen to provide nuclei for cavitation to take place and hence higher cavitational yield is obtained.

Some important design aspects of steam bubble cavitation in water pool, in acoustic cavitation device and with a hydrodynamic cavitation device are concluded below

Steam condensation regimes determine the steam jet formation and its breakup into steam bubble. To get higher cavitational yield, the steam condensation regimes (steam flux and pool temperature) should be chosen such that, as soon as the steam leaves the nozzle it immediately detaches itself from the issuing jet and forms a bubble. For low steam fluxes (<100 kg m^2 s) pool temperature should be lesser than 50°C to operate in transient chugging (TC) regime to get higher cavitational yield.

Collapse pressure and temperature was seen to increase with an increase in the liquid pool temperature. But very high liquid pool temperatures would reduce the number of independent steam bubbles being injected into water and hence it would lower the cavitational yield. Maximum number of steam bubble is obtained in the liquid pool temperature of 40 to 50°C.

Generating smaller steam bubbles in acoustic cavitation device can improve the efficiency of the cavitation process.

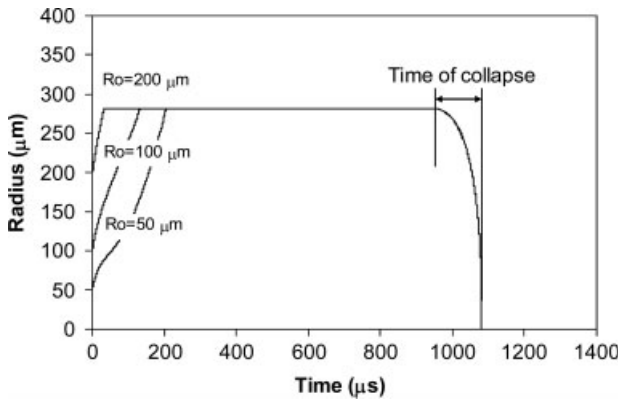

Figure 14. Simulated radius history of steam bubble of different initial sizes injected after cavitating device when operated at cavitation number = 1.

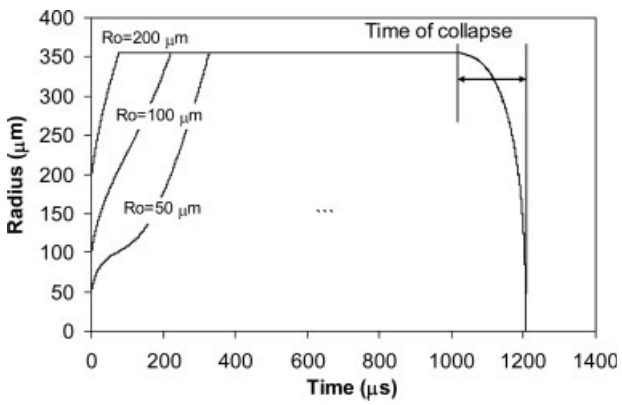

Figure 15. Simulated radius history of steam bubble of different initial sizes injected after cavitating device when operated at cavitation number = 2.

Table 4. Collapse Pressure (atm) and Temperature (K) of Steam Bubbles After Cavitating Device

	Cavitation Number = 1		Cavitation Number = 2	
Initial Size	Collapse Pressure (atm)	Collapse Temperature (K)	Collapse Pressure (atm)	Collapse Temperature (K)
50	4032	2265.159	3857.156	2324.69
100	4037.199	2265.499	3858.079	2324.76
200	4044.314	2265.993	3859.367	2324.855

In the case of steam injection near a cavitating device the size of a steam bubble can be controlled by altering the liquid turbulence (shear).

Introducing steam near a cavitating device shears steam bubbles of size larger than the critical size into smaller ones. This increases the overall cavitational yield due to larger number of cavitational events. Hydrodynamic cavitation and steam cavitation would synergistically work to give enhanced cavitational yield without actually reaching the hydrodynamic cavitating conditions (cavitation number) < 1.0).

Notation

C_v = cavitation number
C = velocity of sound in liquid phase
D_{AB} = diffusivity of species A into B
d = diameter
f_T = turbulence frequency
g = acceleration due to gravity
h = local heat transfer coefficient
K = thermal conductivity
l = boundary layer thickness
l_R = length of recovery zone after orifice plate
l_{eddy} = turbulent length scale
m = moles of the bubble
$\dot{m}$ = rate of mass transfer from/to the cavity
n = number of holes/ openings in orifice plate
M = molecular weight
Nu_D = Nusselt number based on bubble dynamics
Nu_T = Nusselt number based on turbulence
P = pressure
P_1 = inlet pressure, pressure at the upstream of orifice
P_2 = outlet pressure at the downstream of orifice
Pe = Peclet number
P^O = vapor pressure
Pr = Prandtl number
P_m = power dissipated per unit mass of liquid in recovery zone
P_v = partial pressure of vapor in bubble
Q = heat transfer rate due to conduction
R = radius of bubble
Re = Reynolds number
R_g = Ideal gas law constant
S = bubble wall velocity
T = temperature
t = time
U = internal energy associated with incoming/outgoing mass
V = liquid velocity in cavitating device i.e. orifice plate
v = velocity
W = PV kind of work done on cavity
We = Weber number
z = potential head associated with incoming/outgoing mass
ρ = density
α = thermal diffusivity
α_c = accommodation coefficient
μ = viscosity of liquid
σ = surface tension

Subscript

avg = average
B = bubble
∞ = liquid at infinity
l = liquid phase
int = bubble liquid interface
th = thermal
m = mass transfer
o = orifice
p = pipe

Superscript

$'$ = fluctuating

Literature Cited

1. Jyoti KK, Pandit AB. Water disinfection by acoustic and hydrodynamic cavitation. *Biochem Eng J*. 2001;7:201–212.
2. Sivakumar M, Pandit AB. Wastewater treatment: a novel energy efficient hydrodynamic cavitational technique. *Ultrason Sonochem*. 2002;9:123–131.
3. Ambulgekar GV, Samant SD, Pandit AB. Oxidation of alkylarenes to the corresponding acids using aqueous potassium permanganate by hydrodynamic cavitation. *Ultrason Sonochem*. 2004;11:191–196.
4. Ambulgekar GV, Samant SD, Pandit AB. Oxidation of alkylarenes using aqueous potassium permanganate under cavitation: comparison of acoustic and hydrodynamic techniques. *Ultrason Sonochem*. 2005;12:85–90.
5. Kozyuk OV. Use of hydrodynamic cavitation for emulsifying and homogenizing processes. *Am Lab*. 1999;31:6–8.
6. Pandit AB, Joshi JB. Hydrolysis of fatty oils: effect of cavitation. *Chem Eng Sci*. 1993;48:3440–3442.
7. Save SS, Pandit AB, Joshi JB. Microbial cell disruption: role of cavitation. *Chem Eng J Biochem Eng J*. 1994;55:B67-B72.
8. Chivate MM, Pandit AB. Effect of sonic and hydrodynamic cavitation on aqueous polymeric solutions. *Ind Chem Eng*. 1993;35:52–57.
9. Rayleigh L. On the pressure developed in a liquid during the collapse of a spherical cavity. *Philanthropic Mag*. 1917;34:94–98.
10. Plesset MS. The Dynamics of Cavitation Bubbles. *ASME J Appl Mech*. 1948;16:228–231.
11. Shima A, Tomita Y. The Behaviour of a spherical bubble in mercury. Report 2. Rep. Inst. High Speed Mech., 1979;39, Tohoku Univ., Tohoku, Japan 19.
12. Moholkar VS, Senthilkumar P, Pandit AB. Hydrodynamic cavitation for sonochemical effects. *J Histochem Cytochem*. 1999;47:53–65.
13. Toegel R, Gompf B, Pecha R, Lohse D. Does water vapor prevent upscaling sonoluminescence? *Phys Rev Lett*. 2000;85:3165–3168.
14. Yasui K. Alternative model of single-bubble sonoluminescence. *Phys Rev E*. 1997;56:6750–6760.
15. Nigmatulin RI, Khabeev NS, Nagiev FB. Dynamics, heat and mass transfer of vapour-gas bubbles in a liquid. *Int J Heat Mass Transf*. 1981;24:1033–1044.
16. Hertz H. *Ann Phys*. 1882;17:177.
17. Langmuir I. *Phys Rev*. 1913;2:329.
18. Knudsen M. *Annals of Physics*. 1915;47:197.
19. Schrage R. W. *A Theoretical Study of Interface Mass Transfer*. New York: Columbia University Press, 1953.
20. Ytrehus T, Østmo S. Kinetic theory approach to interphase processes. *Int J Multiphase Flow*. 1996;22:133–155.
21. Moholkar VS, Pandit AB. Bubble behavior in hydrodynamic cavitation: effect of turbulence. *AIChE J*. 1997;43:1641–1648.
22. Bird RB, Stewart WE, Lightfoot EN. *Transport phenomena*, 2nd ed. New York: Wiley, 2002. Chap 5, pp 157.
23. Gogate PR, Pandit AB. Engineering design methods for cavitation reactors II: hydrodynamic cavitation. *AIChE J*. 2000;46:1641–1649.
24. Lewis DA, Davidson JF. Bubble sizes produced by shear and turbulence in a bubble column. *Chem Eng Sci*. 1983;38:161–167.

25. Whitaker S. Forced convection heat transfer correlations for flow in pipes, past flat plates, single cylinders, single spheres, and for flow in packed beds and tube bundles. *AIChE J*. 1972;18:361–371.
26. Hirschfelder JO, Curtiss CF, Bird RB. *Molecular Theory of Gases and Liquids*. New York: Wiley, 1954:539.
27. Gastgar SN. Optimisation of Hybrid cavitation, M. Chem. Eng. Thesis, Mumbai University, Mumbai, India 2004.
28. Weissler A, Cooper HW, Snyder S. Chemical effect of ultrasonic waves: oxidation of potassium iodide solution by carbon tetrachloride. *J Am Chem Soc*. 1950;72:1769–1775.
29. Naidu Prasad DV, Rajan R, Kumar R, Gandhi KS, Arakeri VH. Modelling of a batch sonochemical reactor. *Chem Eng Sci*. 1994; 49:877–888.
30. Kerney PJ, Faeth GM, Olson DR. Penetration characteristics of a submerged steam jet. *AIChE J*. 1972;18:548–553.
31. Chan CK, Lee CKB. Regime map for direct contact condensation. *Int J Multiphase Flow*. 1982;8:11–20.
32. Chun MH, Kim YS, Park JW. An investigation of direct condensation of steam jet in subcooled water. *Int Commun Heat Mass Transf*. 1996;23:947–958.
33. Toegel R, Lohse D. Phase diagrams for sonoluminescing bubbles: a comparison between experiment and theory. *J Chem Phys*. 2003; 118:1863–1875.
34. Bapat PS, Pandit AB. Thermodynamic and kinetic considerations of nucleation and stabilization of acoustic cavitation bubbles in water. *Ultrason Sonochem*. 2007;doi:10.1016/j.ultsonch. 2007.01.005.
35. Washburn EW. International critical tables. *McGraw Hill Book Co*. 1928:3:257.
36. Yan Y, Thorpe RB. Flow regime transitions due to cavitation in the flow through an orifice. *Int J Multiphase Flow*. 1990;16:1023–1045.

Appendix A

Sample calculations of turbulent frequency, fluctuating velocities & fluctuating pressure amplitude in case of flow past an orifice for cavitation number (C_v) = 1 (Moholkar and Pandit, 1997)

Inlet Pressure (P1) = 405300 Pa

Downstream Pressure (63% recovery) ($P2$) = 255339 Pa

Pipe Diameter (ID) (d_p) = 0.038 m

Orifice Diameter (d_O) = 0.0055 m

Number of holes in orifice plate (n) = 1

Velocity at orifice (Vo) = 22.4 m/s (from Eq. 24)

Distance after orifice in which pressure recovery takes place (l_R) = $8 \times d_p$ = 0.304 m

Turbulence Length scale (l_{eddy}) = $0.08(dp + do/2)$ = 0.00174 m

Pressure drop across orifice (ΔP) = (P_1–P_2) = 149,961 Pa

Power dissipation per unit mass of liquid (P_m)

$$= \frac{\text{Pressure drop} \times \text{Volumetric Flowrate}}{\text{Mass of liquid in in recovery zone}}$$

$$= \frac{\Delta P \times V_p}{l_R \times \rho_1}$$

= 231 J / kg s

Turbulent fluctuating velocity (V') = $\left(Pm \times l_{eddy}\right)^{0.3}$ = 0.76 m/s

Turbulent frequency (f) = V'/l = 440

Time of pressure recovery (τ) = $\frac{L_R}{(Vo+Vp/2)}$ = 0.026 s

Assuming linear pressure recovery from at time (t = 0) to downstream pressure (P2) in τ s, the pressure can be given as

$$P(t) = P2 + \frac{P2 - P_{vena}}{\tau} t$$

Mean local velocity $V(t)$ can be obtained by applying Bernoulli's principle at various locations downstream the orifice

$$V_t = V_O^2 + \frac{P2 - P(t)}{1/2 \rho_l}$$

The turbulent velocity fluctuation has been superimposed on it by assuming a sinusoidal velocity variation in the instantaneous local velocity with the estimated frequency and is given as

$$V_{td} = V_t - V' Sin(2\pi ft)$$

This instantaneous value of velocity is used to obtain the instantaneous fluctuating pressure by

$$P(t) = P_{vena} + 1/2 \rho l (V_O^2 - V_{td}^2)$$

The figure shows the shows the bulk pressure recovery and turbulent pressure recovery as obtained from above calculations. The value of pressure amplitude is calculated as shown in figure below

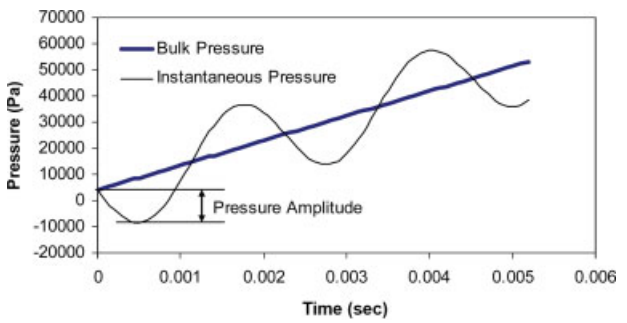

Figure A1. Pressure variation experienced by a travelling cavity.

[Color figure can be viewed in the online issue, which is available at www.interscience.wiley.com.]

Pressure profile calculated as per the calculations shown above.

Manuscript received Apr. 16, 2007, and revision received Feb. 27, 2008.